

Alumina copper composites for thermoelectric applications

Tushar Duryodhanrao Jogi

A Dissertation Submitted to
Indian Institute of Technology Hyderabad
In Partial Fulfillment of the Requirements for
The Degree of Master of Technology



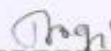
भारतीय प्रौद्योगिकी संस्थान हैदराबाद
Indian Institute of Technology Hyderabad

Department of Materials Science and Metallurgical Engineering,
Indian Institute of Technology Hyderabad

June, 2014

Declaration

I declare that this written submission represents my ideas in my own words, and where others' ideas or words have been included, I have adequately cited and referenced the original sources. I also declare that I have adhered to all principles of academic honesty and integrity and have not misrepresented or fabricated or falsified any idea/data/fact/source in my submission. I understand that any violation of the above will be a cause for disciplinary action by the Institute and can also evoke penal action from the sources that have thus not been properly cited, or from whom proper permission has not been taken when needed.



Tushar Duryodhanrao Jogi

MS12M1003

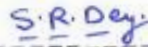
Approval Sheet

This thesis entitled "Alumina nano-particles dispersed copper matrix thermoelectric composites" by Tushar Duryodhanrao Jogi is approved for the degree of Master of Technology from IIT Hyderabad.



Dr. Atul Suresh Deshpande (Examiner)

Assistant Professor



Dr. Suhash Ranjan Dey (Adviser)

Assistant Professor



Dr. Bharat Bhooshan Panigrahi (Co-Adviser)

Assistant Professor

Dr. Debaprasad Shee (Chairman)

Assistant Professor

Acknowledgements

To express my gratitude during my tenure as M. Tech student at IITH, my words have no bounds, but still I will curtail my feelings to few words.

I would like to thank first my thesis advisor **Dr. Suhash Ranjan Dey** and thesis co-adviser **Dr. Bharat Bhooshan Panigrahi** for his endless support and patience to carry out this work. I would also extend my gratitude to HOD of Department of Materials Science and Metallurgical Engineering, **Dr. Pinaki Prasad Bhattacharjee**, to provide with all facilities required for my experiments. I must owe my thanks to **Dr. Ranjith Ramadurai** for helping me in my experiments. Also, I am thankful to **Dr. Saswata Bhattacharya** for his valuable inputs time to time.

This work would not be complete without the incessant moral support from my family members and their sacrifice. Also I am grateful for my friends **Bhalchandra, Rahul, Ankit, Nida** and other M.Tech Scholar for supporting me time to time. I must appreciate **Basant, Sushmita, Md. Zaid, Mallesh, Rajkumar, Saj Mohan, Sudarshan** and all other PHD scholars for their consistent help in carrying out my experiment.

The last but not least, those who help me unknowingly and I miss them to quote their name, to carry out this work, my heart is filled with gratitude for them

Dedicated to

MY FAMILY

My Father: D. Y. Jogi

My Mother: Jyoti Jogi

My beloved Sister: Tejaswini

Abstract

The composite of the Copper (APS 25 μm) and Alumina (APS 20 μm and APS 5 μm) is synthesized using pressureless sintering at 900 $^{\circ}\text{C}$. The composite with fine alumina particles dispersed in copper matrix has higher resistivity and Seebeck coefficient as that of coarse alumina dispersed copper matrix composite. Also density achieved for fine and coarse alumina dispersed in copper matrix is 94% and 93% respectively. The sample for PLD deposition is produced of composition Cu+5wt% coarse alumina using pressureless sintering at 1000 $^{\circ}\text{C}$. After the sintering of PLD sample 95% density is achieved. The Seebeck coefficient of composite suddenly increases at 500 $^{\circ}\text{C}$ which may ascribed to oxidation of copper. The pulsed laser deposition is done at substrate temperature of 200 $^{\circ}\text{C}$ on alumina substrate. The average grain size obtained of the film is 7 μm . There is reduction in the atomic fraction of copper in the film as that of in the target.

Nomenclature

SEM – Scanning Electron Microscopy

PLD – Pulsed Laser Deposition

TPM – Thermopower Measurement

EDS – Electron Dispersive X-ray Spectroscopy

CIP – Cold Isostatic Pressing

XRD – X-ray Diffraction

APS – Average Particle Size

AR – As received

Contents

Declaration	Error! Bookmark not defined.
Approval Sheet	Error! Bookmark not defined.
Acknowledgements	4
Abstract.....	6
Nomenclature	7
Introduction	10
1.1 Overview.....	10
Literature Review	12
2.1 Seebeck Effect	12
2.2 Thermoelectric Figure of Merit.....	16
2.3 Patent Review	19
2.4 Novelty of the present work	20
Experimental Process.....	21
3.1 Starting Material	21
3.2 Grinding and mixing.....	21
3.3 Precompaction	21
3.4 CIP	22
3.5 Pressureless Sintering	22
3.6 Cutting of TPM sample.....	23
3.7 Characterization	23
3.7.1 SEM Imaging.....	23
3.7.2 Density Measurement.....	23
3.7.3 Seebeck coefficient and resistivity measurement	24
3.8 Pulsed Laser Deposition(PLD)	24
3.8.1 Sample Preparation.....	24
3.8.2 Density measurement	24
3.8.3 Deposition	24
3.9 Characterization of PLD films	25
3.10 Experimental Process Flowchart.....	26
Results & Discussion	27
4.1 Starting Materials	27
4.1.1 Particle Size Measurement.....	30

4.1.2	Crystallite Size Measurement.....	30
4.2	TPM Samples.....	31
4.2.1	Precompaction	31
4.2.2	CIP	33
4.2.3	Pressureless Sintering	34
4.2.4	Density Measurement.....	35
4.2.5	Seebeck Coefficient and Resistivity measurement	35
4.3	PLD sample.....	39
4.3.1	Precompaction	39
4.3.2	CIP	39
4.3.3	Pressureless Sintering	40
4.3.4	Density Measurement.....	40
4.4	Deposition.....	41
4.5	Discussion	44
	Summary.....	46
	Future Work	47

Chapter 1

Introduction

1.1 Overview

At present the energy resources on earth are depleting day by day gradually. Considering the present scenario the search for alternate energy resources to trap energy and recycling are getting pace. At the same time, emission from industries, automobiles, etc. are becoming alarming and threat to the environment, but emit large amount of heat. This phenomenon soars the cost of energy and worsen the greenhouse effect of the earth. If this thermal energy being emitted could be trapped and reutilized by any means, it can be economically and environmentally beneficial. The thermoelectric effect (namely Seebeck effect) can be one of the alternate way to trap the thermal energy loss. The Seebeck effect converts the thermal energy into electrical energy. The thermoelectric power generators made of thermoelectric material are solid state devices with no moving parts they are silent, reliable and

scalable and making them ideal for small, distributed power generation [1]. This additional harnessing will not only improve efficiencies of thermal power plants but also it will reduce pollution with reducing fuel consumption. The widely used thermoelectric materials are most semiconductors like Bi_2Te_3 , PdTe , Si-Ge alloys etc. [2]. But these materials are economically non-viable to produce to be used for large quantity application and have been long inefficient. There is need to develop other cost effective and economically viable materials and their production method. There are various approaches to improve the performance of the thermoelectric materials. Nanostructure engineering is one of the approaches. The present work is done extending the idea of nanostructure engineering.

Chapter 2

Literature Review

2.1 Seebeck Effect

The first evidence of the thermoelectric effect was observed by T. J. Seebeck in 1821 [3]. He demonstrated one of the first thermoelectric effects, namely Seebeck Effect, as shown in Figure 2-1. The Seebeck effect can be

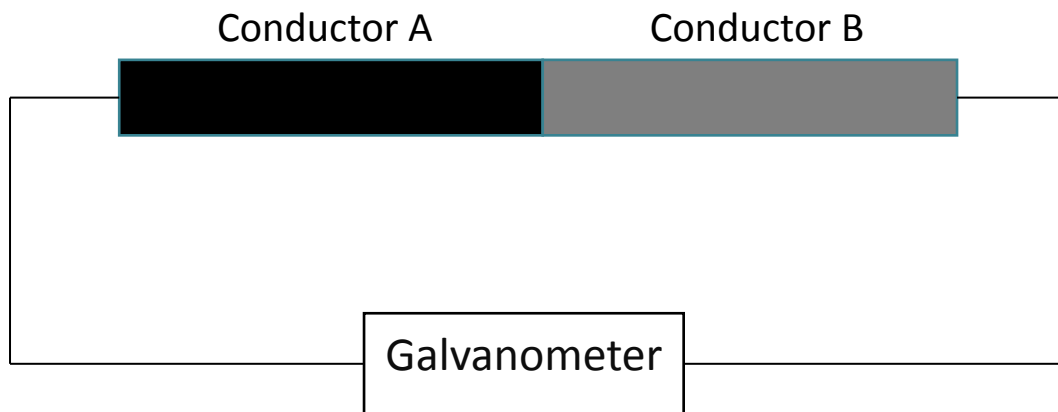


Figure 2-2: Schematic of Seebeck Effect

demonstrated by connecting the wires of different metals (e.g. copper and aluminum wires). The other ends of the wire should be connected to a galvanometer or the sensitive voltmeter. If the junction of two wires is heated, it is observed that meter shows a small voltage. The junction of two wires forms a thermocouple. It is also observed that magnitude of voltage developed across the junction, known as thermoelectric voltage is

proportional to the temperature gradient across junction. Suppose that temperature ΔT is established between two junctions and the other ends of the conductor A and B are maintained at same temperature then it is generally found that potential difference will appear between free ends. The Seebeck Coefficient which is defined as potential difference developed across the two conductor because of heating of the junction per unit temperature difference [3].

The Seebeck coefficient (α) is given as:

$$\alpha = \frac{V}{\Delta T}$$

By convention, the sign of S represents the potential of cold side with respect to hot side. If electron diffuses from hot side to cold side, cold side is negative with respect to hot side and Seebeck coefficient is negative.

The highest occupied energy level at absolute zero temperature is Fermi energy (E_F). At absolute zero temperature probability of occupying all energies lower than E_F will be one i.e. $f(E) = 1$. At finite temperature electrons tends to occupy energies higher than E_F .

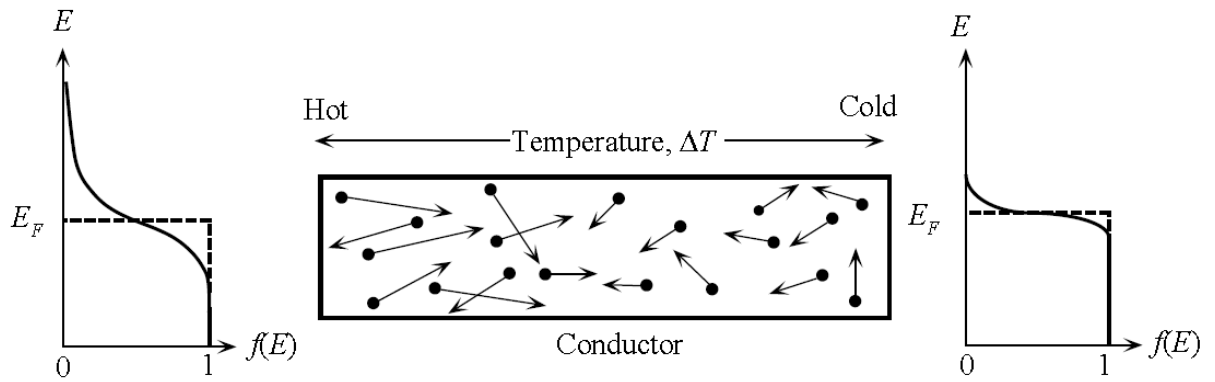


Figure 2-2: Electron diffusion during Seebeck effect [4]

It means the average energy of an electron increases with increase in temperature. That means the hot end of the conductor extends to have higher average energy than that of cold. It means the electron in hot have higher mean speed and mean free path will be higher in hot end as that of cold end. Consequently the more energetic electrons in hot end diffuse towards cold region until potential difference V is developed which prevent further diffusion (refer figure 2-2) [4].

The net migration of electron from hot to cold or cold to hot end is determined by energy dependence of electron concentration, mean free path and mean scattering time [4]. If mean free path increases strongly with energy then electrons will diffuse from hot end to cold end and Seebeck coefficient will be negative. If mean free path decreases strongly with energy,

electrons migrate from cold to hot end and Seebeck coefficient is positive.

These conclusions are valid only for metals.

For efficient thermoelectric materials, the Seebeck coefficient should be large (absolute value should be large). To ensure the Seebeck coefficient is large, there should be single type of charge carrier. The inter-relationship between the Seebeck coefficient and charge carrier is given by [5]:

$$S = \frac{8\pi^2 k^2}{3eh^2} m^* T \left(\frac{\pi}{3n} \right)^{2/3}$$

where k : Boltzmann's constant; m^* : effective mass; n : charge carrier density.

From above equation, it is evident that the Seebeck coefficient is inversely proportional to charge carrier density. The charge carrier density of metals is very high (in range of $10^{28} / \text{m}^{-3}$). Semiconductors have higher charge carrier densities than ceramic materials. It means that the metals, semiconductor and ceramic have increasing Seebeck coefficient respectively. But at the same time they have decreasing electrical conductivity which may be degrading for thermoelectric materials. Then the obvious choice of material would be semiconductor which have optimized Seebeck coefficient and electrical conductivity or combination of metal and ceramic. The right choice of metal and ceramic needed to be studied to get good thermoelectric material.

2.2 Thermoelectric Figure of Merit

The Seebeck coefficient is a number which determines the usefulness of thermoelectric material. Under the given temperature difference, the ability of material to produce electric power is quantified by thermopower factor which is given as:

$$\mathbf{thermopower\ factor = \sigma S^2}$$

where σ : electrical conductivity

But the power factor may not indicate how efficiently the material generates electric power. The ability of given material to efficiently generate electric power is given by dimensionless figure of merit (ZT).

$$\mathbf{ZT = \frac{S^2 \sigma T}{\kappa}}$$

where κ : thermal conductivity(W/m/K)

Thus, from the expression for dimensionless figure of merit it is clear that for the thermoelectric material to be efficient, it should have high Seebeck coefficient, high electrical conductivity and lower thermal conductivity.

The variation of electrical conductivity, thermal conductivity and Seebeck coefficient and figure of merit with respect to carrier concentration is as shown in figure 2-3 [6]. From the figure it can be deduced that

semiconductor are best thermoelectric materials having higher ZT values.

The materials which are best thermoelectric materials are bismuth telluride (Bi_2Te_3), lead telluride

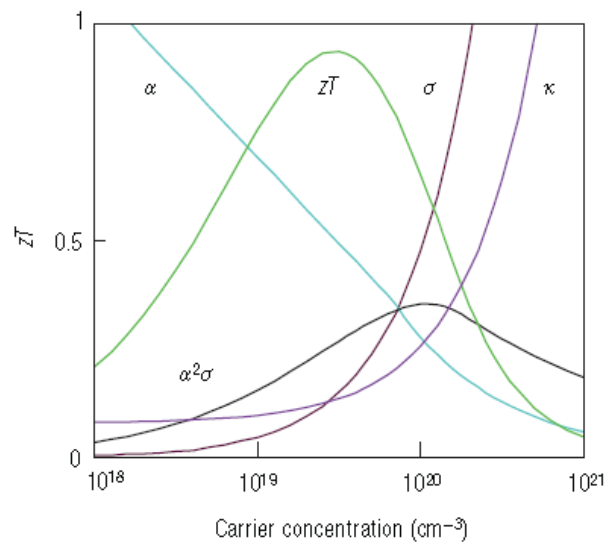


Figure 2-3: Variation of thermoelectric properties with charge carrier concentration [6]

(PbTe), which are not economically viable to be used for large quantity applications. There is a need to develop other cost effective and commercially viable materials and their production methods. This has led to the development of not only various other types of thermoelectric materials (Skutterudites, Clathrates, oxides, etc.) but also restructuring of the existing thermoelectric materials into multi-layer materials, nano-composites, nano-wires, quantum dots, etc.[2,3]. To increase the performance (i.e., figure of merit) of the thermoelectric materials, attempts are made to enhance their

electrical conductivity and/or to reduce their thermal conductivity. Various strategies adopted so far are:

- a) Introducing distortion in the unit cell to reduce the thermal conductivity without seriously affecting the electrical conductivity.
- b) Resonant scattering by localized rattling atoms: weakly bonded foreign ions (for example rare earth material) in oversized atomic cage formed by other atoms (base material) which gives rise to localized incoherent vibrations and reduces the thermal conductivity.
- c) Multilayer substructure approach or superlattice approach.
- d) Refining the crystallographic grain size/particle size in multiphase system, i.e. nanostructure approach.

In the nanostructure approach of reducing the crystallographic grain size into nano-scale, there is a reduction of both thermal and electronic conductivities due to augmentation of grain boundaries. However, the electronic conductivity can be enhanced by introducing more coherent interfaces and the grain boundary scattering of electrons can be reduced. And, in the nanostructure approach of lowering the particle phase size to nanometer level in the multiphase system, the thermal conductivity is reduced by phonon scattering (having longer mean free path in order of

hundreds of nanometers) at the interphase boundaries. Whereas, electrons having shorter mean free paths in the order of several nanometers, scatter less at the interphase boundaries, largely preserving its electrical conductivity.

2.3 Patent Review

Recently the nano-composite of alumina and nickel and other metals having high electrical conductivity and high Seebeck coefficient and low thermal conductivity is claimed to be developed, which can be used at high temperatures (shown in figure 2-4) [8].

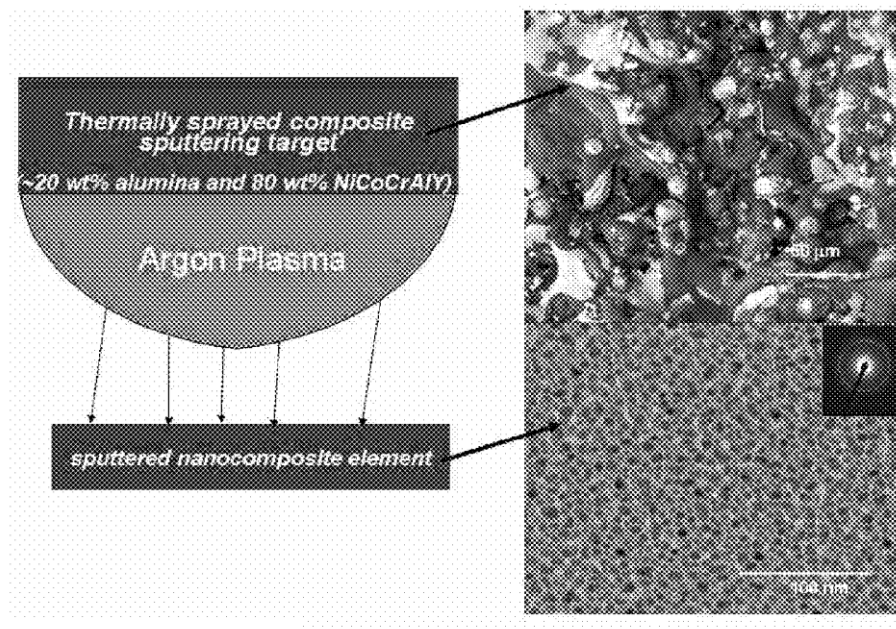


Figure 2-4: Nano-composite of Alumina and Nickel and other metals [8]

2.4 Novelty of the present work

Till now high ZT value thermoelectric materials are mainly semiconductors and are not cost effective to be used for bulk scale applications. Ideal thermoelectric materials would be ceramics having good electrical conductivity. We propose a novel idea of utilizing the electrical conductive metallic materials in ceramics of high Seebeck values, by mixing them methodically to obtain high thermoelectric power. Advantage of using powdered materials route is to have greater control over composition and homogeneity of phase distribution. At the nano-scale, electron confinement not only increases the density of states at the Fermi level but also increases the phonon scattering at the metal-ceramic interface, which further augments the ZT values. This route is expected to lead to an economical production and would be useful to convert the waste heat exhaust from the thermal plants into electricity for auxiliary usages, in turn increasing the electric generation efficiency of the thermal plants.

Chapter 3

Experimental Process

3.1 Starting Material

The starting material for present work is metal and ceramic. The choice of metal highly conductor of electricity and choice of ceramic is low conductor of heat. The metal chosen is Copper (Alfa Aesar made, 99% pure, -325 mesh 10%max +325 mesh) and ceramic is Aluminum Oxide. The aluminum oxide with two different average particle size has been taken.

3.2 Grinding and mixing

The copper powder and aluminum oxide powders are properly grinded and mixed with the help of Agate mortar and pestle. The mixture of Cu+5wt% Al₂O₃ is prepared. The sample of mentioned composition is prepared for coarse and fine Al₂O₃.

3.3 Precompaction

The precompaction of the properly mixed sample of Cu+5wt% Al₂O₃ is done using the Uniaxial Compression unit. The two sort of cylindrical samples are precompacted. One of 10mm diameter and other of 20mm diameter. 13 grams of powder (13grams each of Cu+5wt% coarse alumina and Cu+5wt% fine alumina) is used for 10mm diameter samples and 5 grams of powder for 20 mm diameter samples (13 grams each of Cu+5wt% coarse Al₂O₃ and Cu+5wt% fine Al₂O₃).

3.4 CIP

The precompacted powder samples are pressed using Cold Isostatic Pressing at 200 MPa for 1 min. The pressure of 2000bar (200MPa) build up in 3 minutes and pressure release time is 2 min.

3.5 Pressureless Sintering

The samples after cold isostatic pressing are heated in tubular furnace in Ar+10% H₂ gas. The sintering is done at 900 °C [9]. The heating cycle followed as shown in Figure 3-1. The samples are heated at 10⁰C/min. The sample are hold at 900⁰C for 60 mins. The cooling rate followed is 3⁰C/min.

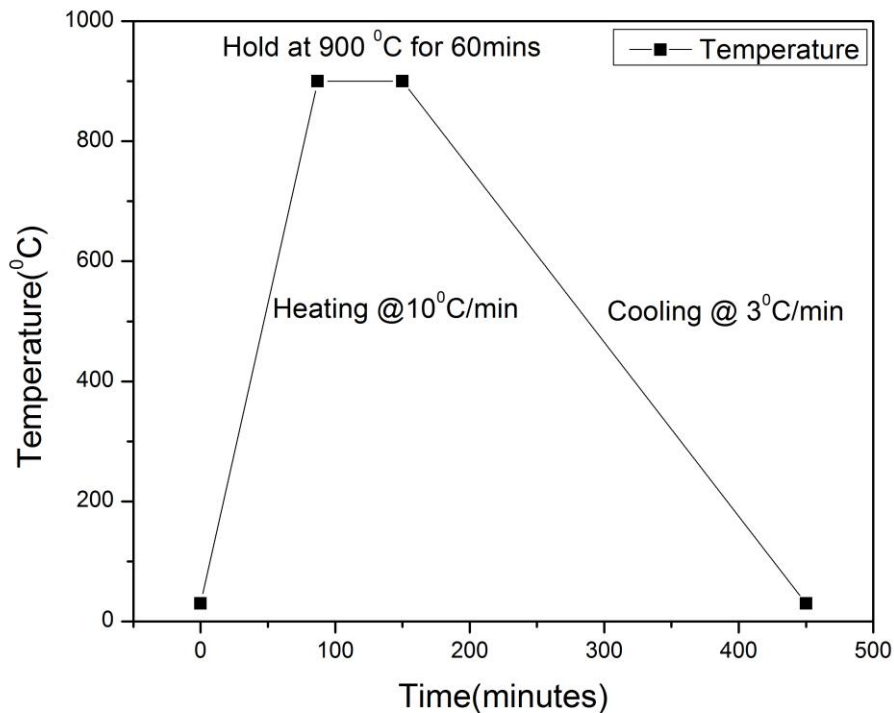


Figure 3-1: Heating Cycle for sintering

3.6 Cutting of TPM sample

The TPM samples obtained after sintering are cut using slow diamond wheel cutter to obtain size of 3mm x 3mm cross section.

3.7 Characterization

3.7.1 SEM Imaging

The Secondary Electron (SE) imaging after precompaction, CIP and sintering is carried out.

3.7.2 Density Measurement

The density measurement after precompaction, CIP and sintering is calculated using Archimedes' principle. The weight of water in beaker is measured on weighing balance (W_{w+b}). The sample is tied with kanthal¹ wire and immersed in the distilled water. Now the weight beaker is measured which has water and sample immersed in water (W_{w+b+s}). The difference ($W_{w+b+s} - W_{w+b}$) will give you the buoyancy force acting on the sample. Also weight of sample is measured in air (W_{sa}). The density of sample (ρ) is calculated as followed.

$$\rho = \frac{W_{sa} \times \text{density of water}}{W_{w+b+s} - W_{w+b}}$$

If the theoretical density of the sample is known then relative density of sample can be calculated after each stage of processing by taking ratio of calculated density to theoretical density of sample.

¹ Kanthal is FeCrAl alloy

3.7.3 Seebeck coefficient and resistivity measurement

The Seebeck coefficient resistivity of sintered sample is measured using instrument of ULVAC-ZEM3 made. The instrument employs four probe method for Seebeck coefficient and resistivity measurement.

3.8 Pulsed Laser Deposition(PLD)

3.8.1 Sample Preparation

The sample preparation for PLD involves the mixing and grinding, precompaction, CIP and pressureless sintering. The precompaction is done at 60 MPa. The CIP is carried out at 200MPa by holding at that pressure for 1 min. The sintering is performed at 1000 °C in Ar+10%H₂ gas for 60 min.

3.8.2 Density measurement

The density of PLD sample is measured after each stage of processing according to section 3.7.2. Further the relative density is computed.

3.8.3 Deposition

The pulsed laser deposition of the samples is performed as per parameters enlisted in table 3.1.

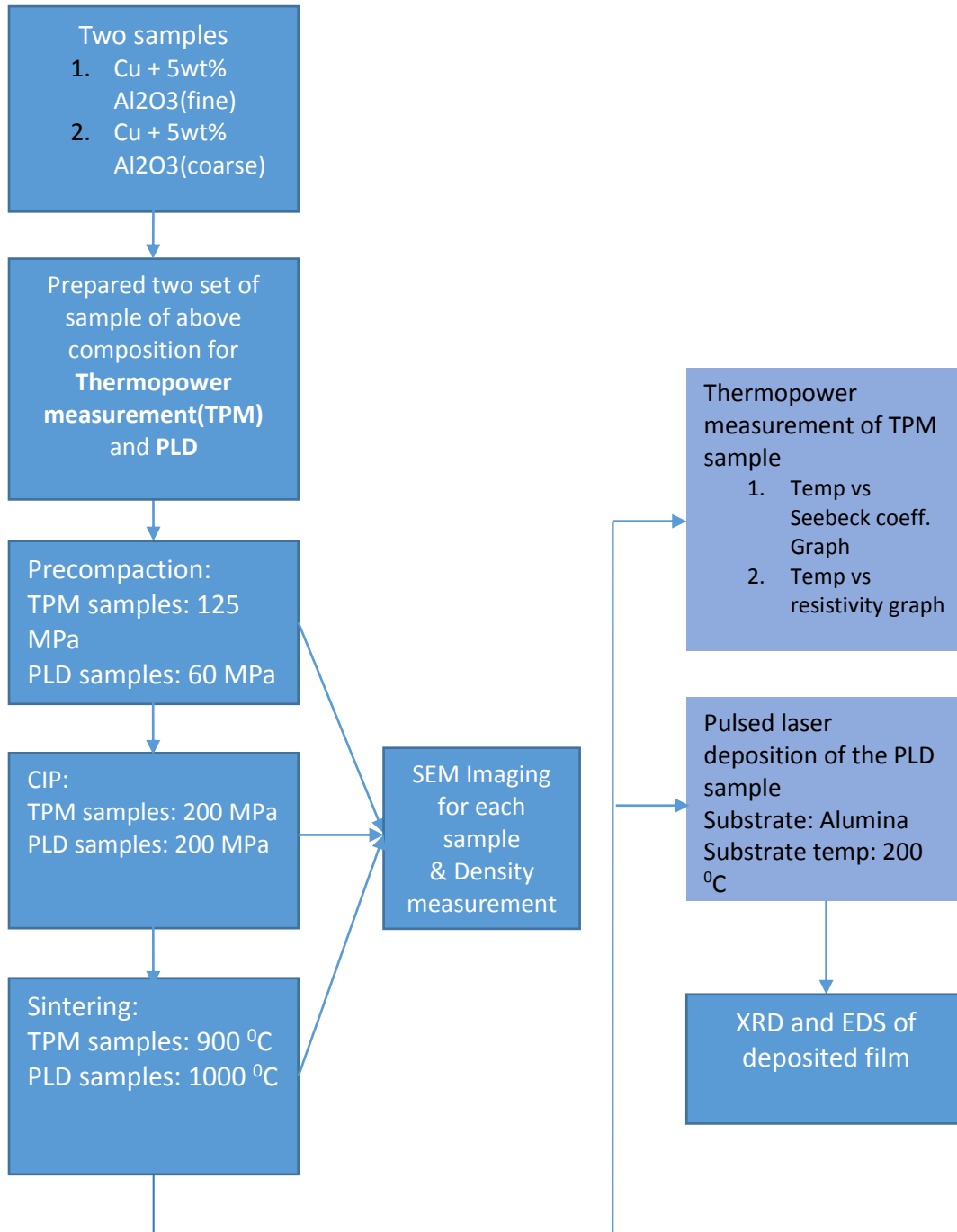
Table 3.1: Parameters for PLD

Repetition rate	3 Hz
Laser Energy	300 mJ
No. of pulses	5400
Deposition time	30 mins
Atmosphere	Vacuum($\sim 10^{-5}$ mbar)
Substrate	Al ₂ O ₃ (5mm x 5mm)
Substrate Temperature	200 °C

3.9 Characterization of PLD films

The deposited film is characterized by XRD and EDS. Also the compositional analysis of film is done through EDS. The compositional changes at the target is also done by EDS.

3.10 Experimental Process Flowchart



Chapter 4

Results & Discussion

4.1 Starting Materials

The starting material Copper and coarse and fine aluminum oxide is characterized using SEM and XRD. The SEM graphs and XRD plots are as shown in Figure 4-1 to 4-3

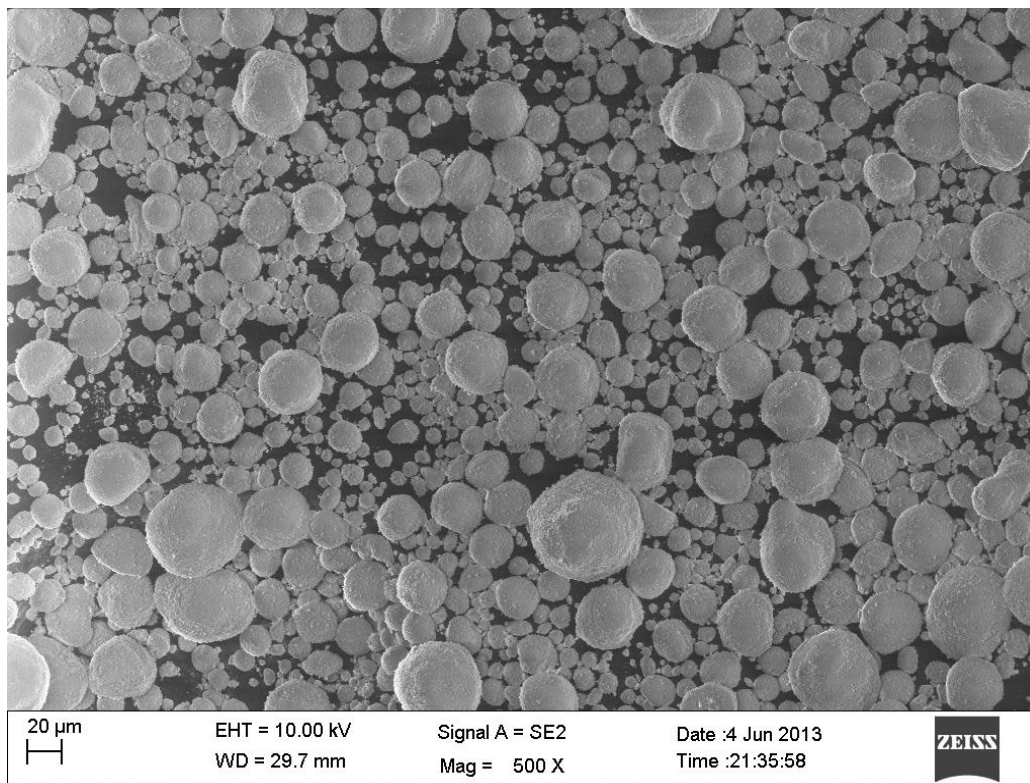


Figure 4-1: SEM micrographs of as received coarse Al_2O_3 powder.

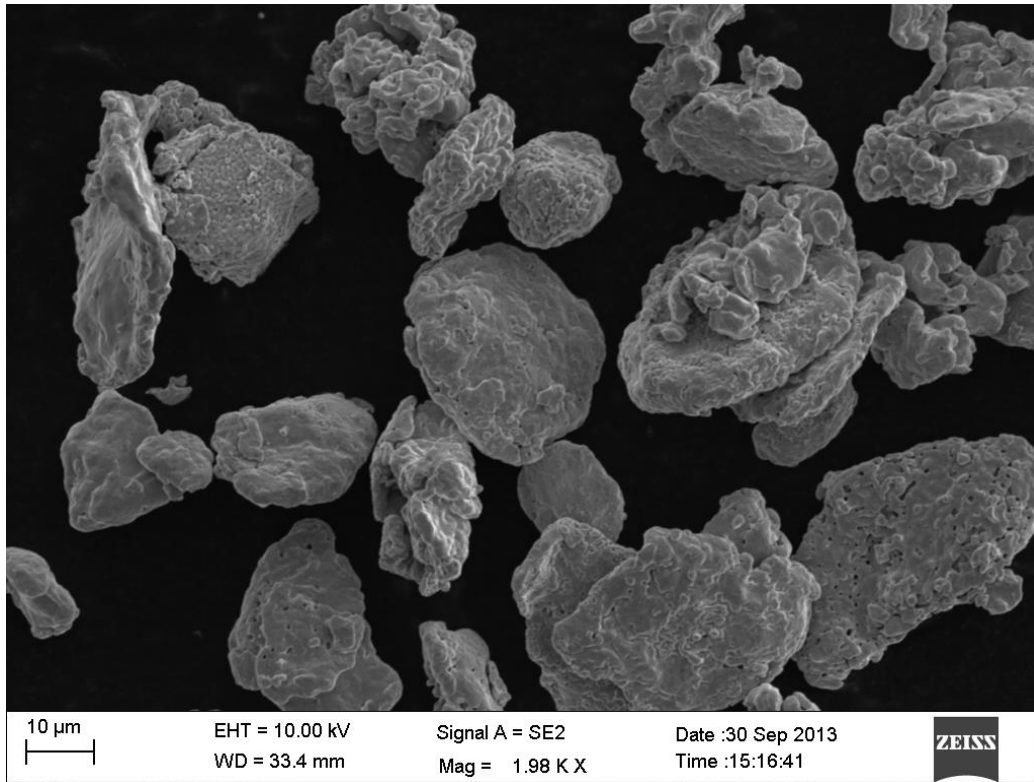


Figure 4-2: SEM micrographs of as received copper powder.

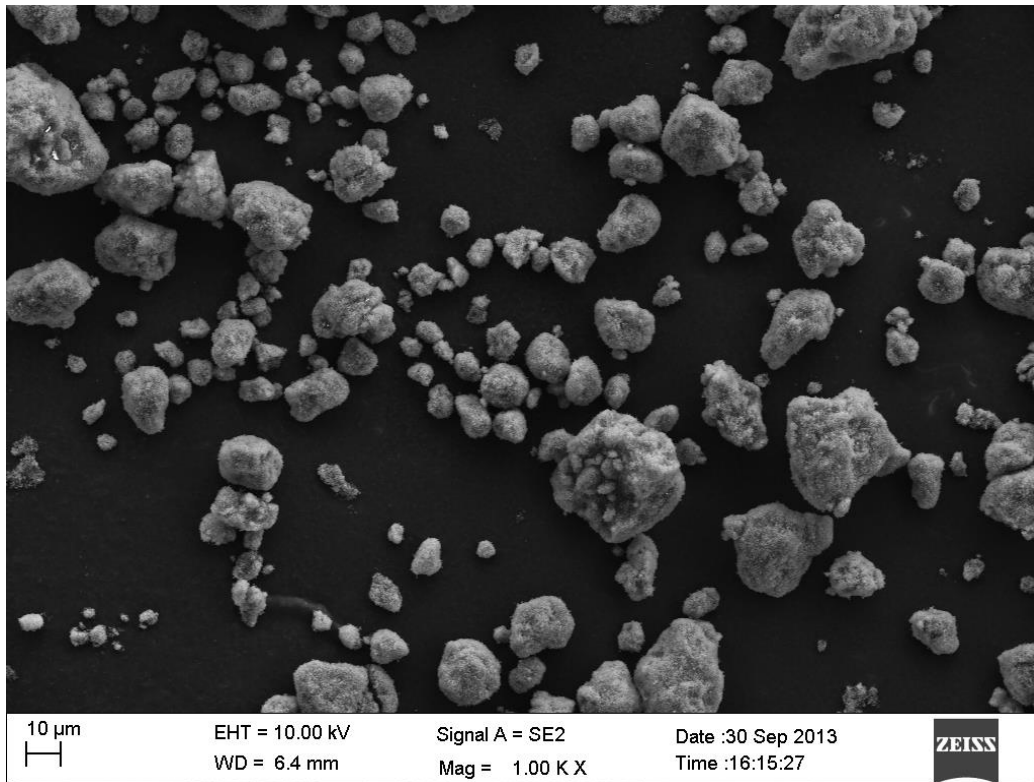


Figure 4-3: SEM micrographs of as received fine Al₂O₃ powder.

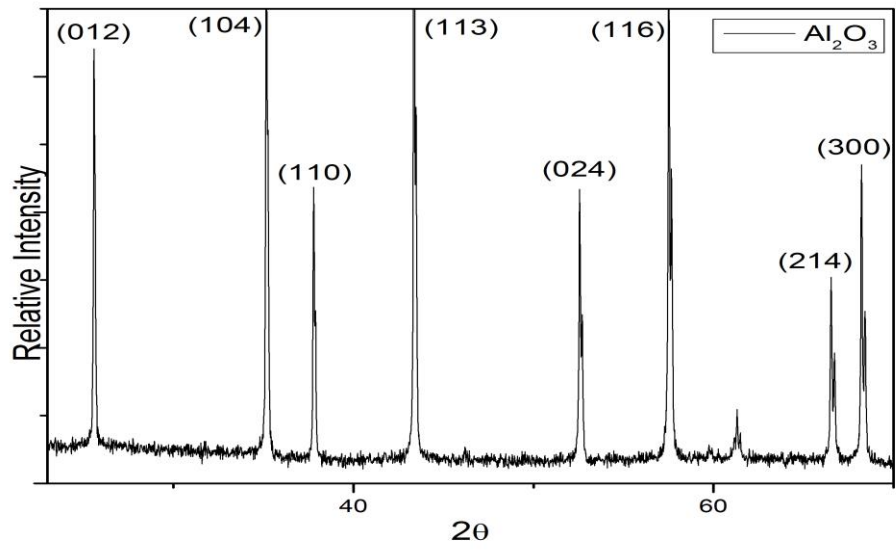


Figure 4-4: XRD plot of as received coarse alumina powder

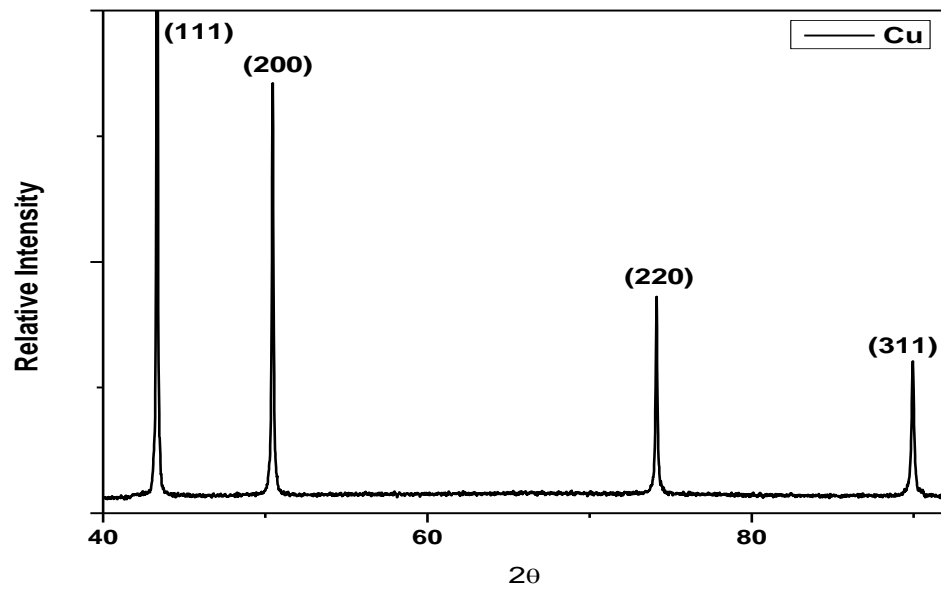


Figure 4-5: XRD plot of as received copper powder

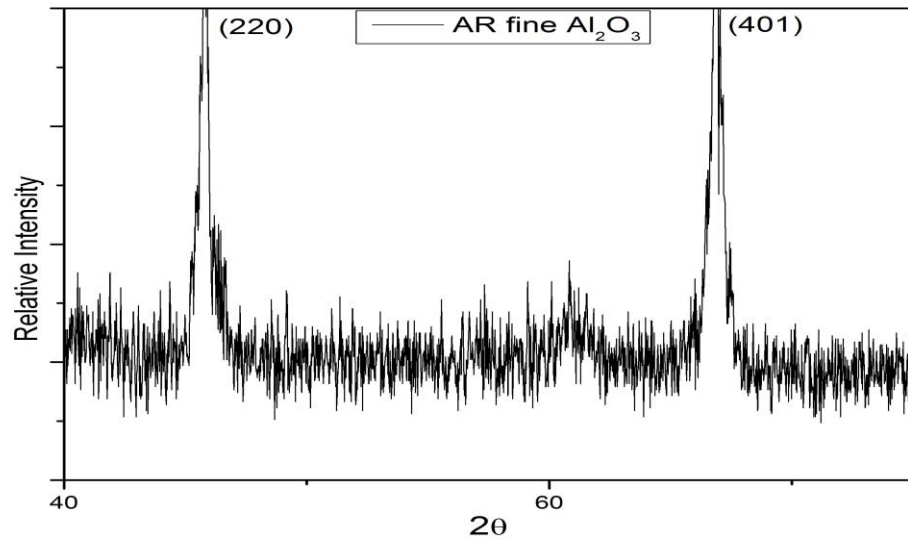


Figure 4-6: XRD plot of as received fine alumina powder

From SEM micrographs in Figure 4-1 to 4-3, it is observed that coarse alumina particles are almost spherical, copper and fine alumina particles are irregular shaped. Comparing the XRD plot in figure 4-4 with JCPDS no. 893072, it is confirmed to be alumina having rhombo-centered crystal structure. Comparing the XRD plot in figure 4-5 with JCPDS no. 892838, it is confirmed to be copper with FCC crystal structure. Comparing the XRD plot in the figure 4-6 with JCPDS no 881609, it is confirmed to be alumina with tetragonal crystal system.

4.1.1 Particle Size Measurement

The particle size is calculated by Martin's diameter [10]. The particle sizes of starting material is as shown in table 4-1.

4.1.2 Crystallite Size Measurement

The crystallite size is calculated by Williamson-Hall method [11]. The crystallite sizes are tabulated in table 4-1.

Table 4-1: Average particle sizes and crystallite size of starting material

Material	APS	Crystallite Size
Copper	25 μm	9 μm
Aluminum oxide(fine)	5 μm	28 nm
Aluminum oxide(coarse)	20 μm	7 μm

4.2 TPM Samples

4.2.1 Precompaction

The SEM micrograph & elemental mapping of precompacted samples are as shown in figure 4-7.

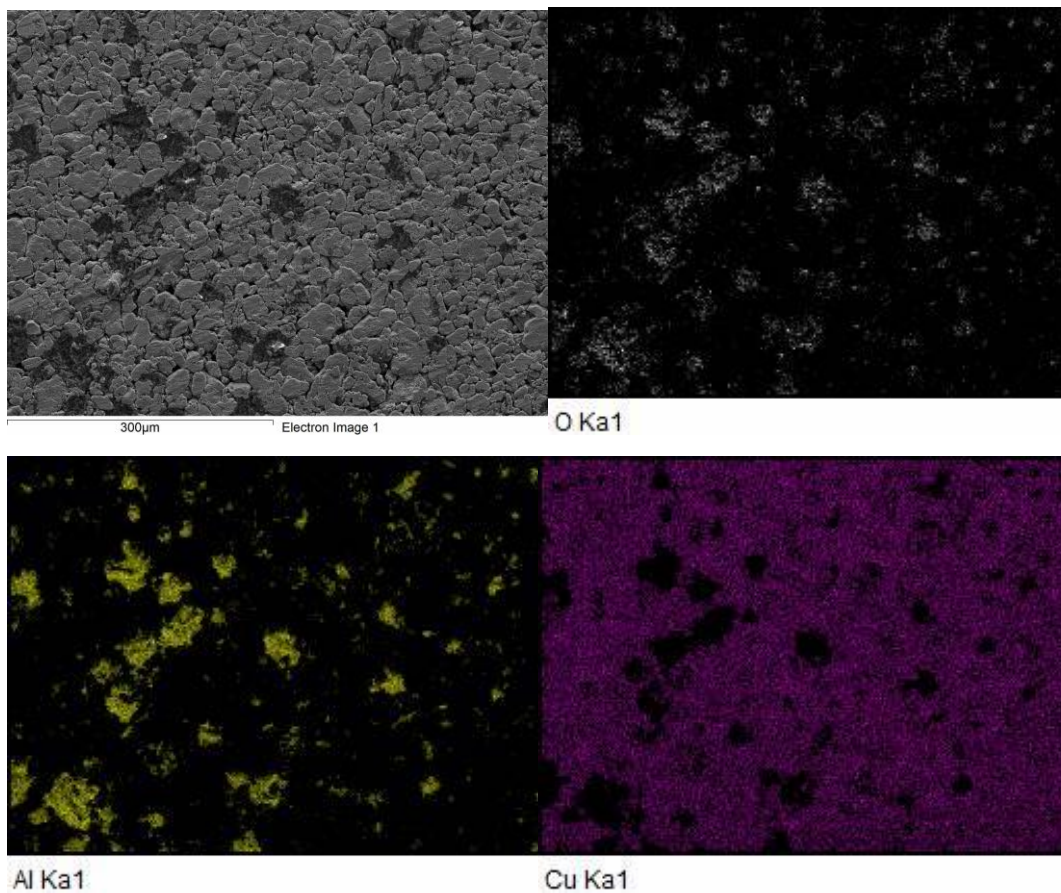


Figure 4-7: SEM micrograph of Cu+5wt% coarse Al_2O_3 after precompaction & elemental mapping

The darker region is Aluminum oxide and brighter region is copper. The SEM micrographs in figure 4-8 shows precompactd Cu+5wt% fine Al₂O₃. In figure 4-8, alumina particles are covered over copper particle as compared to figure 4-4 in which alumina particles are dispersed in between the copper particles. In both figure 4-4 and 4-5 the large amount of voids are observed. Also the copper particles are observed to be oxidized.

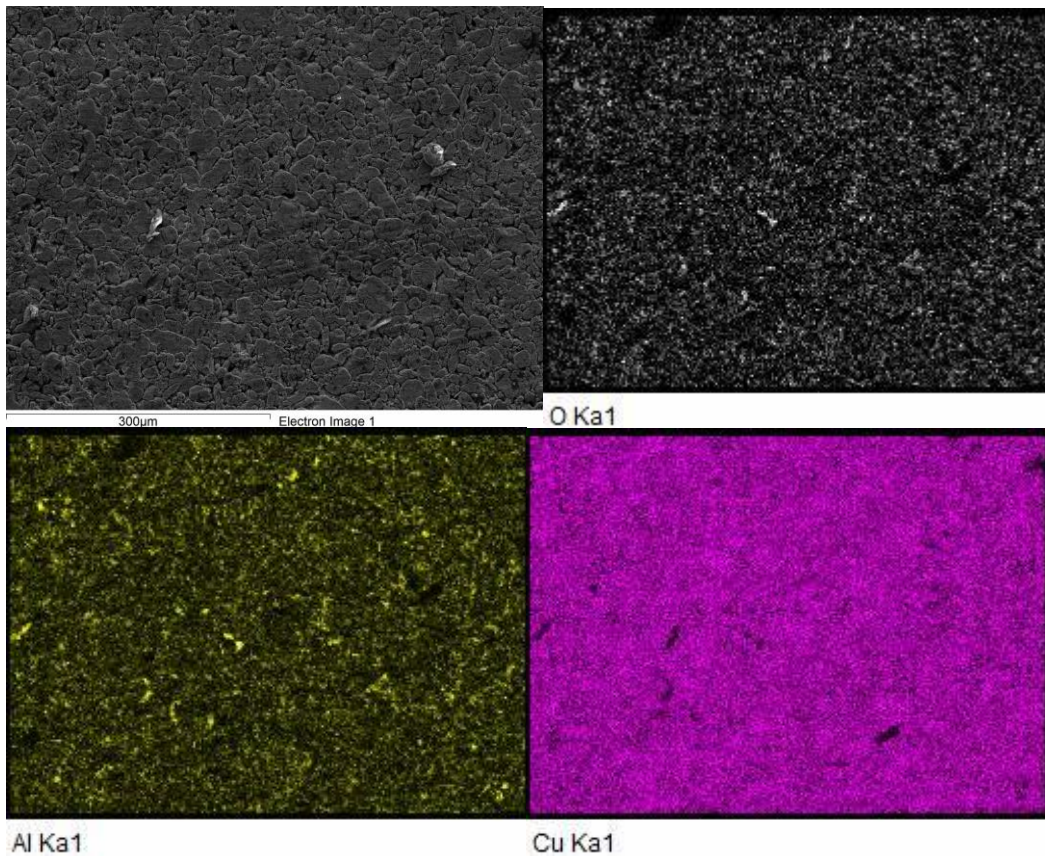


Figure 4-8: SEM micrograph of the Cu+ 5wt% fine Al₂O₃ after precompaction & elemental mapping

4.2.2 CIP

Figure 4-6 shows SEM micrographs of Cu+5wt% coarse alumina after CIP. The necking between the copper particles is observed (encircled in the figure 4-6).

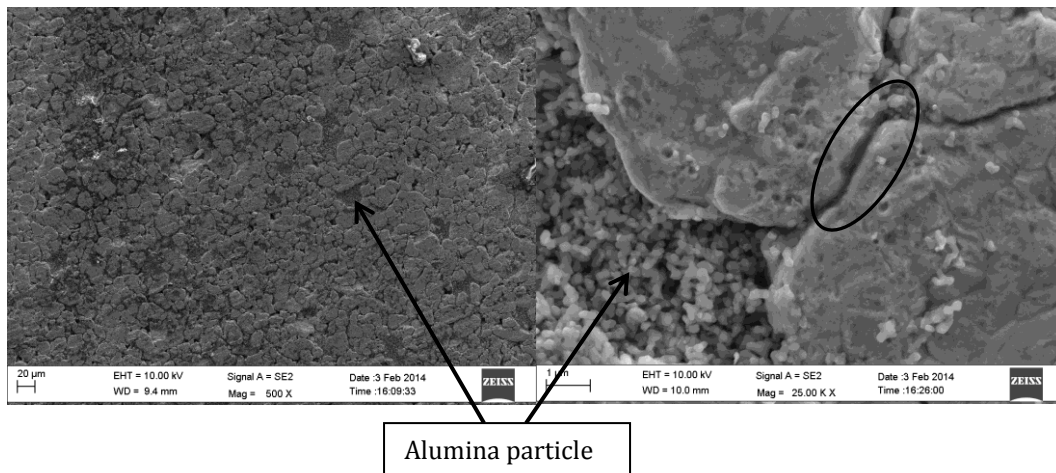


Figure 4-9: SEM micrographs of Cu+5wt% coarse alumina after CIP

Figure 4-7 indicates SEM micrographs of Cu+ 5wt% fine Al_2O_3 . Darker regions denotes the alumina particles. SEM micrographs depicts large number of voids present in the composite.

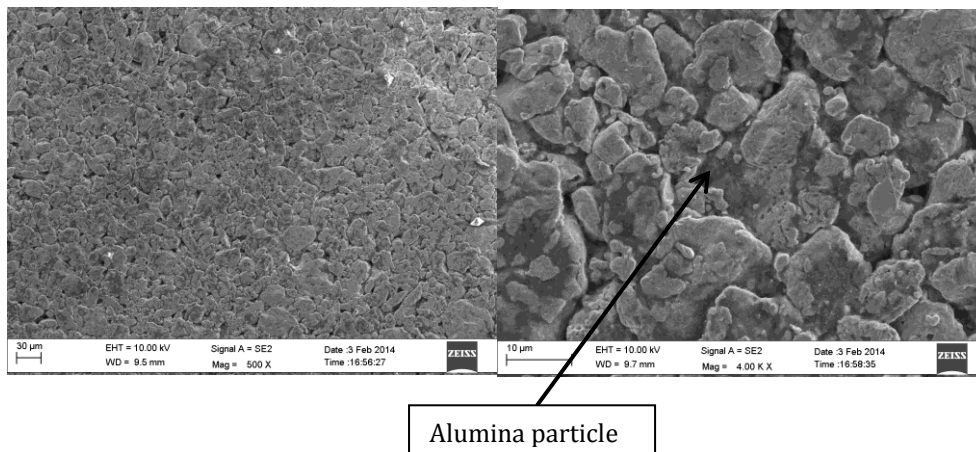


Figure 4-10: SEM micrographs of Cu+5wt% Al_2O_3 after CIP

4.2.3 Pressureless Sintering

Figure 4-8 depicts the SEM micrographs of Cu+5wt% coarse Al_2O_3 after sintering at 900°C in Ar+10% H_2 gas for 60 minutes.

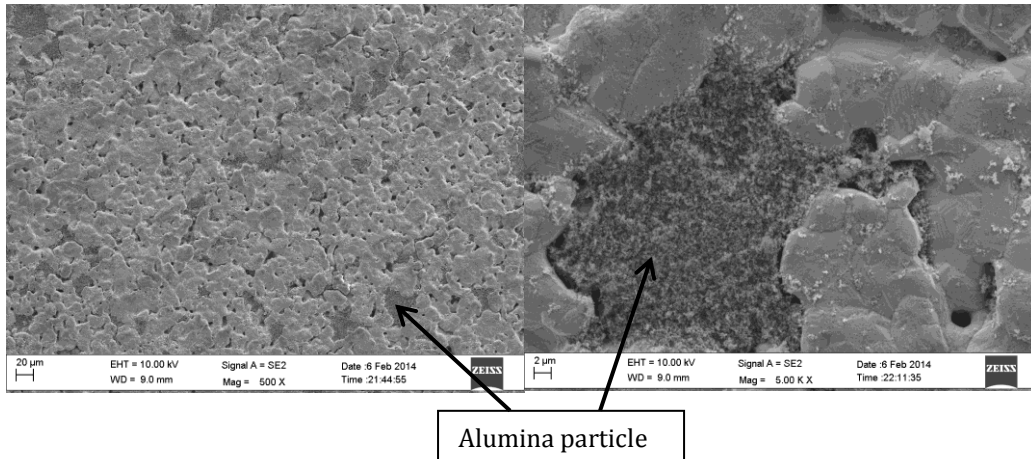


Figure 4-11: SEM micrographs of Cu+5wt% coarse Al_2O_3 after sintering

In the figure 4-8, void contraction can be observed. The darker regions indicates the alumina particles surrounded by copper matrix. Figure 4-9 shows the sintered sample of composition Cu+ 5wt% fine Al_2O_3 covered on copper particles.

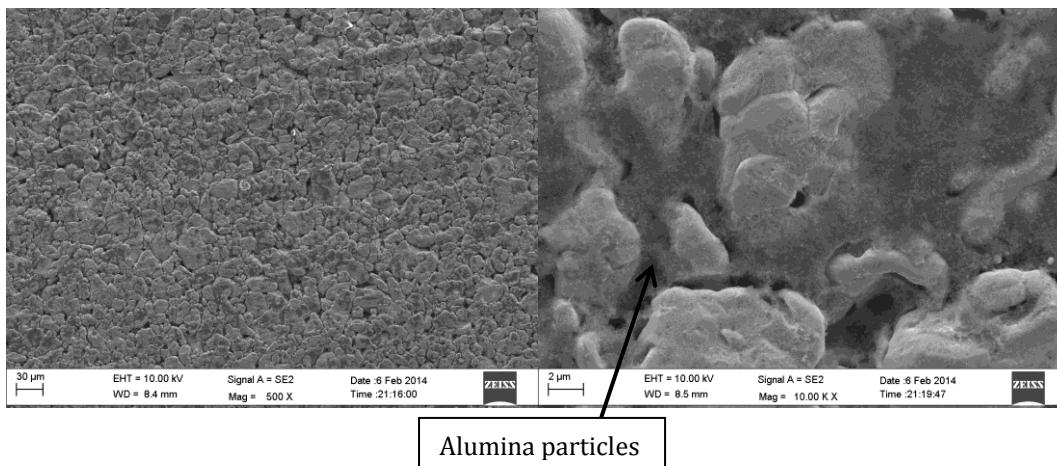


Figure 4-12: SEM micrographs of Cu + 5wt% fine Al_2O_3 after sintering

4.2.4 Density Measurement

The relative density is calculated by measuring the density at every processing step i.e. after precompaction, CIP and sintering. The theoretical density of the composite (Cu+5wt% Al₂O₃) is calculated from the theoretical densities of copper and alumina. The theoretical densities of copper and alumina are 8.941 g/cc and 3.987 g/cc [12]. The theoretical density of Cu + 5wt% Al₂O₃ composite, considering zero volume of voids, is. The calculated percentage relative density at each stage of processing is as tabulated in table 4-2.

Table 4-2: Percentage relative densities of after each stage of processing

	Cu + 5wt% coarse Al ₂ O ₃	Cu + 5wt% fine Al ₂ O ₃
Precompaction	78 %	77 %
CIP	79 %	78 %
Sintering	93 %	94 %

4.2.5 Seebeck Coefficient and Resistivity measurement

The variation of Seebeck coefficient and resistivity with respect to temperature (50 °C to 500 °C) for Cu + 5wt% coarse Al₂O₃ is as shown in figure 4-13 and 4-14 respectively. For composition Cu + 5wt% fine Al₂O₃ is as shown in figure 4-15 and 4-16. Increase in resistivity and Seebeck coefficient with temperature is observed. The sudden increase in Seebeck coefficient for both composite is observed at 500 °C. The figure 4-17 and 4-18 depicts the variation of thermopower factor with respect to temperature for Cu+5wt% coarse Al₂O₃ and Cu+5wt% fine Al₂O₃.

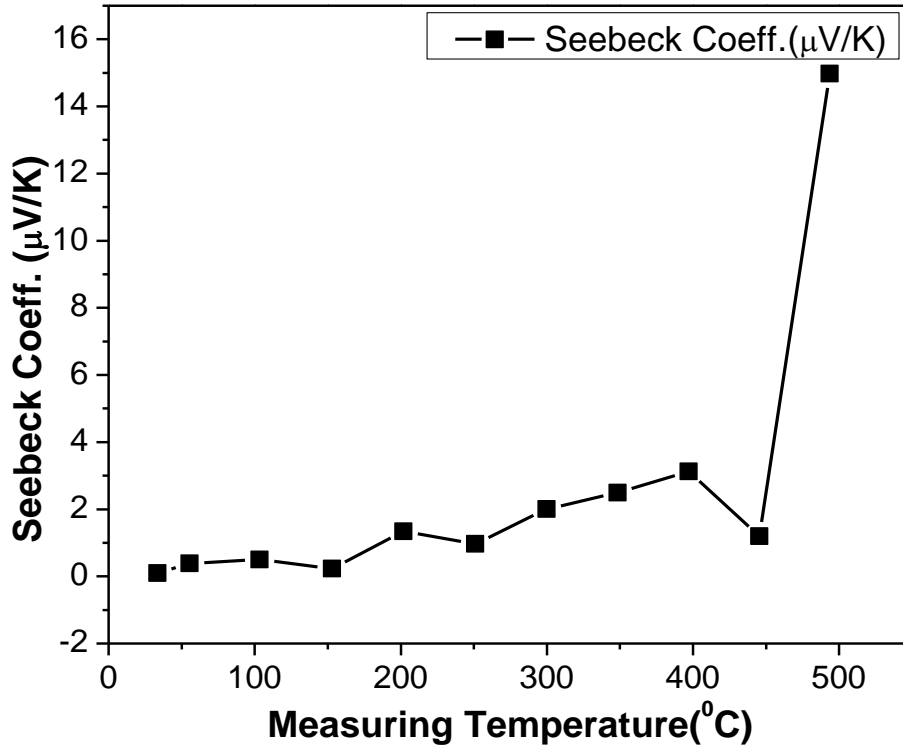


Figure 4-13: Variation of Seebeck Coefficient with temperature of Cu+5wt% coarse Al₂O₃.

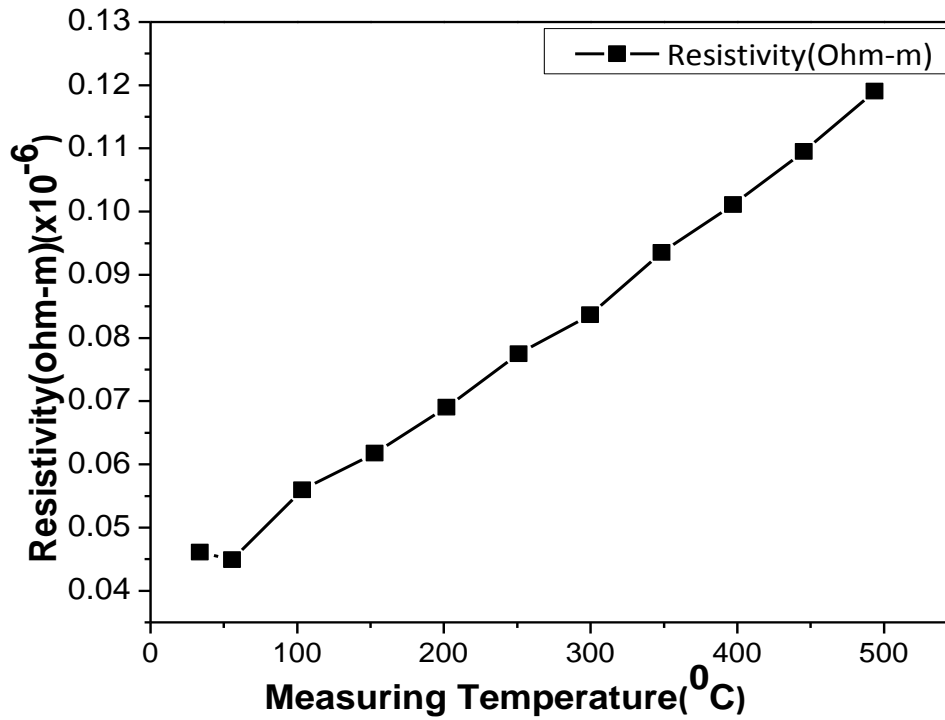


Figure 4-14: Variation of Resistivity with temperature of Cu+5wt% coarse Al₂O₃.

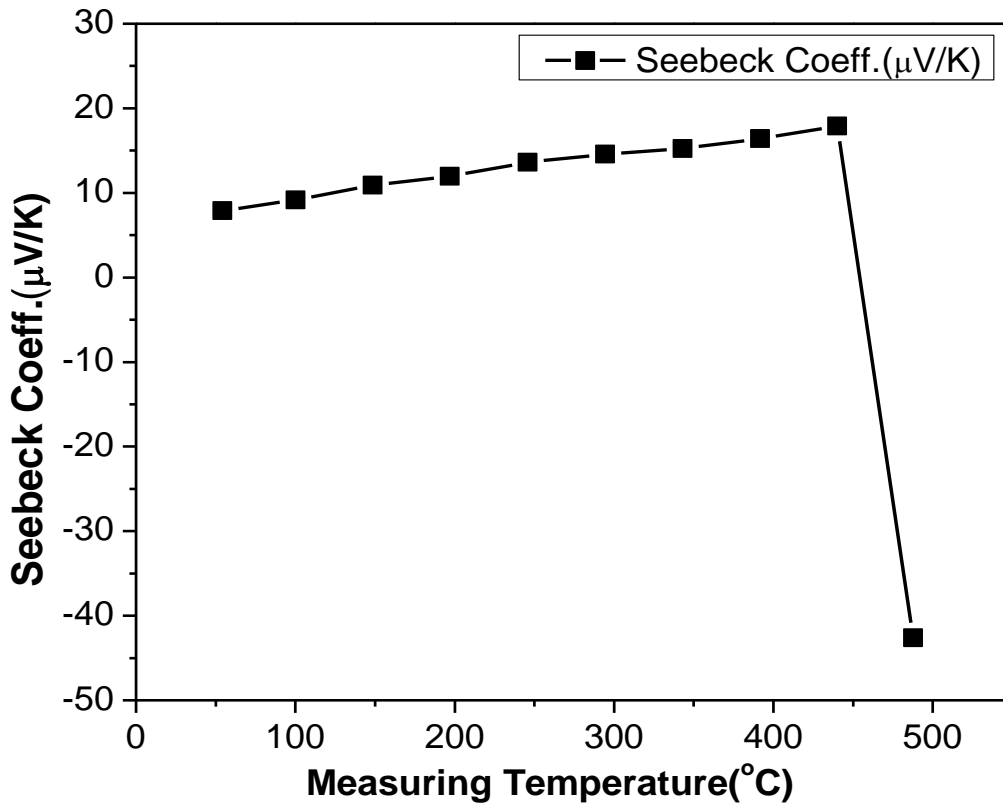


Figure 4-15: Variation of Seebeck coefficient with temperature of Cu+5wt% fine Al₂O₃.

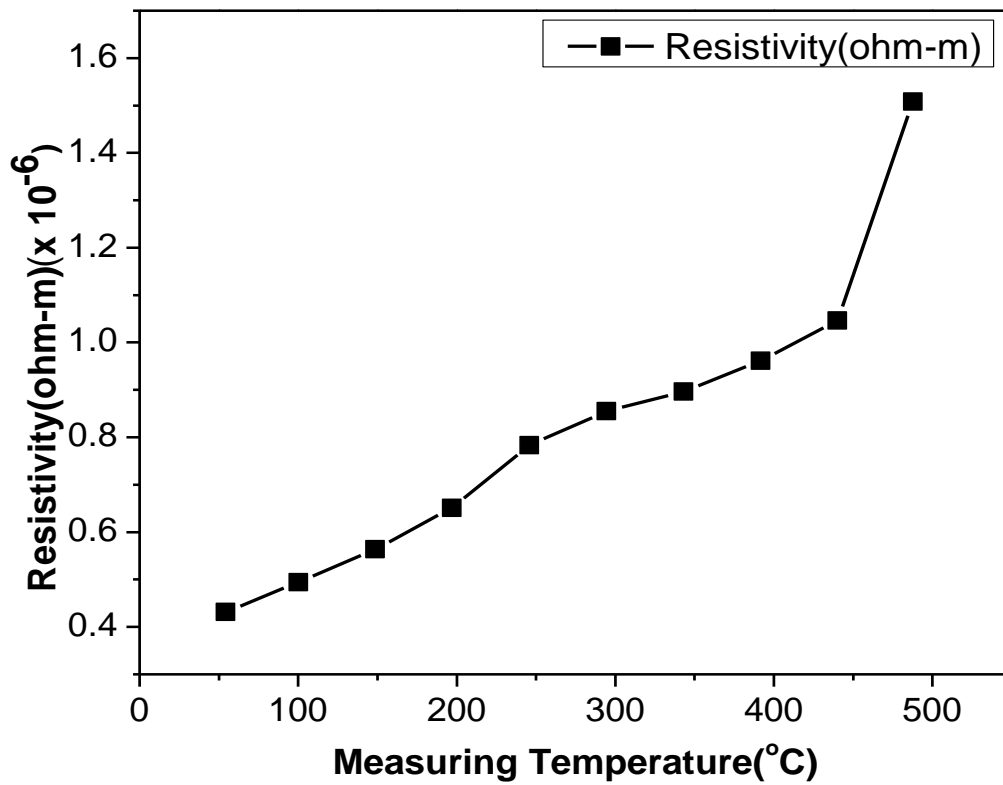


Figure 4-16: Variation of resistivity with temperature of Cu+5wt% fine Al₂O₃.

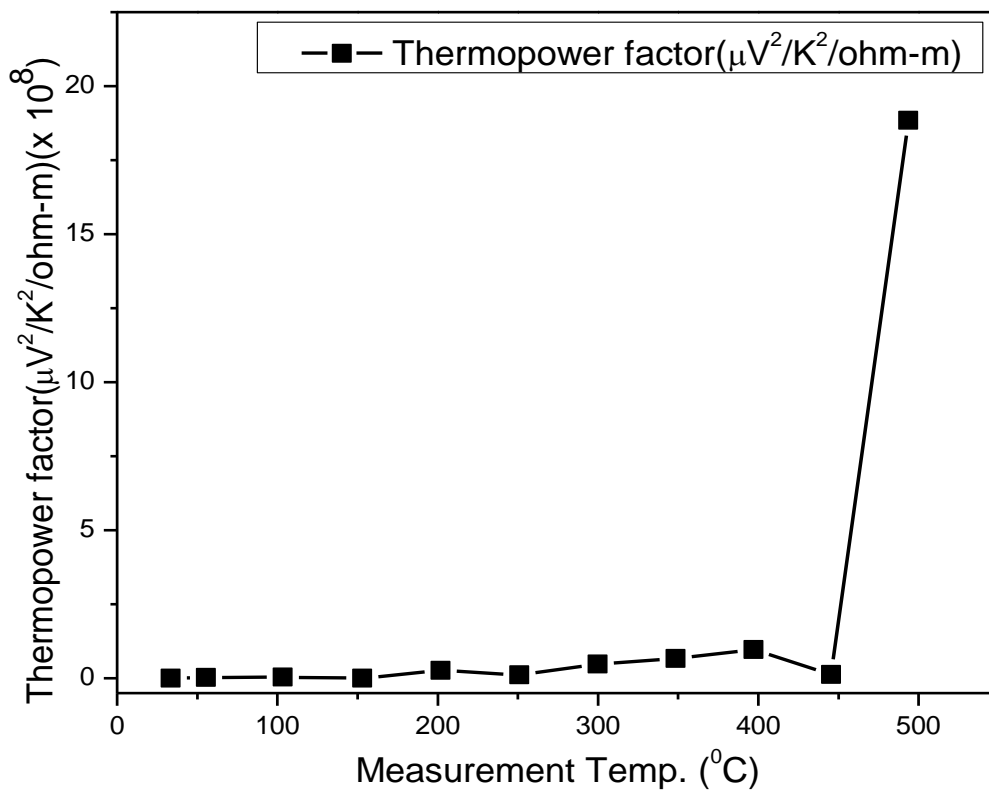


Figure 4-17: Variation of thermopower factor with temperature of Cu+5wt% coarse Al₂O₃.

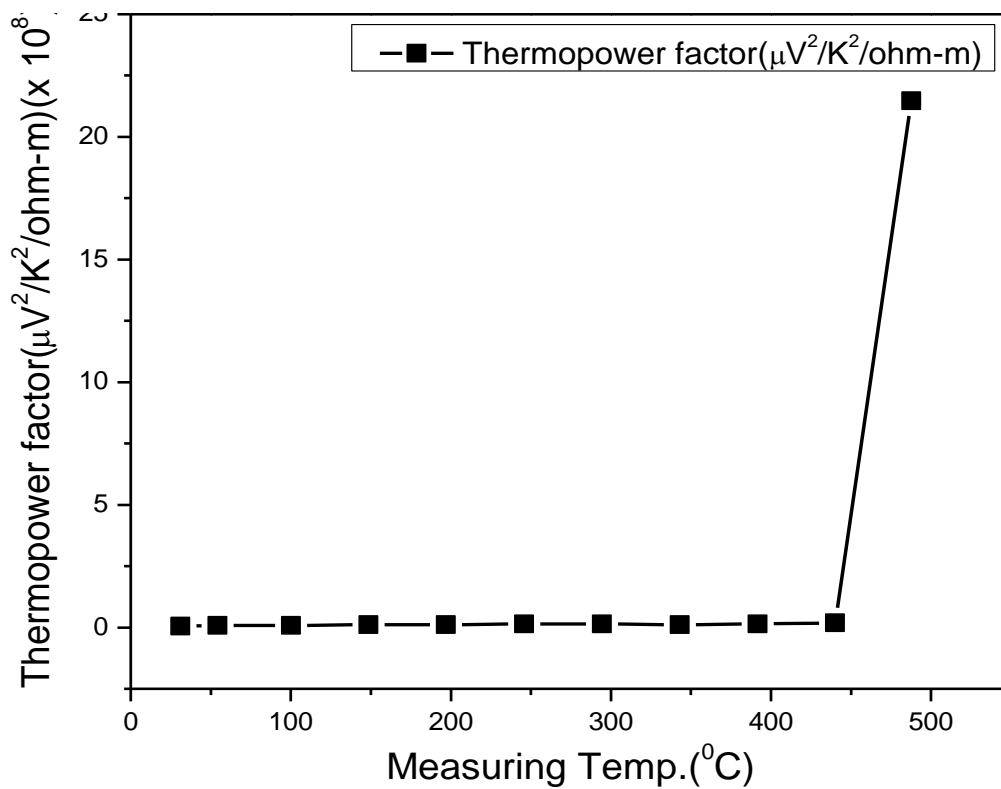


Figure 4-18: Variation of thermopower factor with temperature of Cu+5wt% fine Al₂O₃.

4.3 PLD sample

4.3.1 Precompaction

The figure 4-14 depicts Cu + 5wt% coarse Al₂O₃ after precompaction, whereas the figure 4-15 depicts the Cu+5wt% fine Al₂O₃ after compaction.

In figure 4-14, the darker region indicates the aluminum oxide particles surrounded by copper matrix. In figure 4-15, fine aluminum oxide particles are covered over the copper particles.

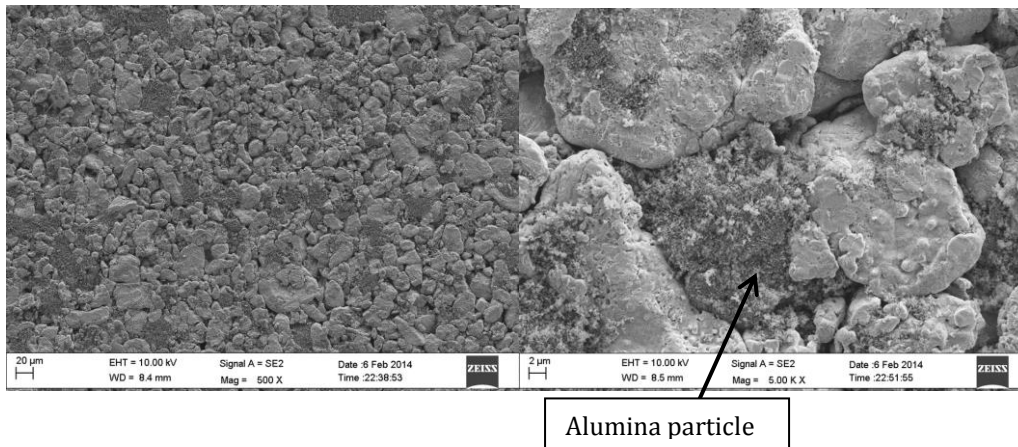


Figure 4-19: SEM micrographs of Cu+5wt% coarse Al₂O₃ after precompaction

4.3.2 CIP

The figure 4-15 depicts the SEM micrographs of Cu+5wt% coarse Al₂O₃ after CIP.

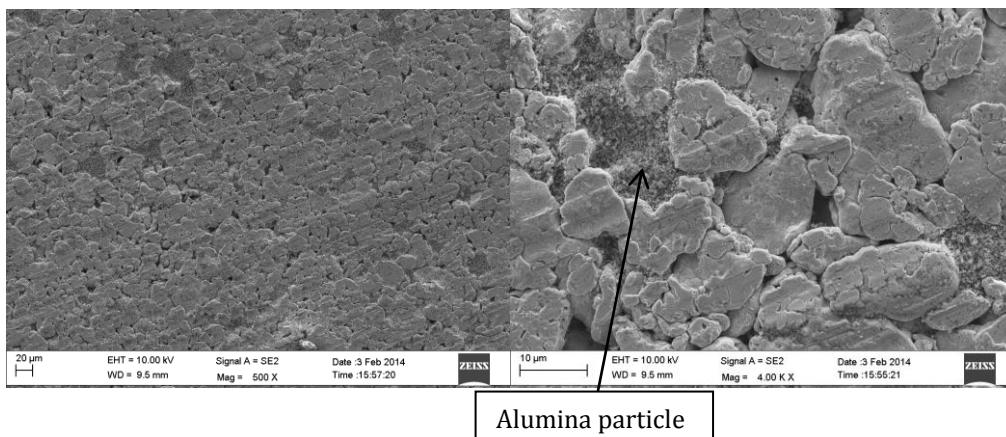


Figure 4-20: SEM micrographs of Cu + 5wt% coarse Al₂O₃ after CIP

4.3.3 Pressureless Sintering

The figure 4-16 depicts SEM micrographs of Cu+5wt% coarse Al₂O₃ after sintering at 1000 °C.

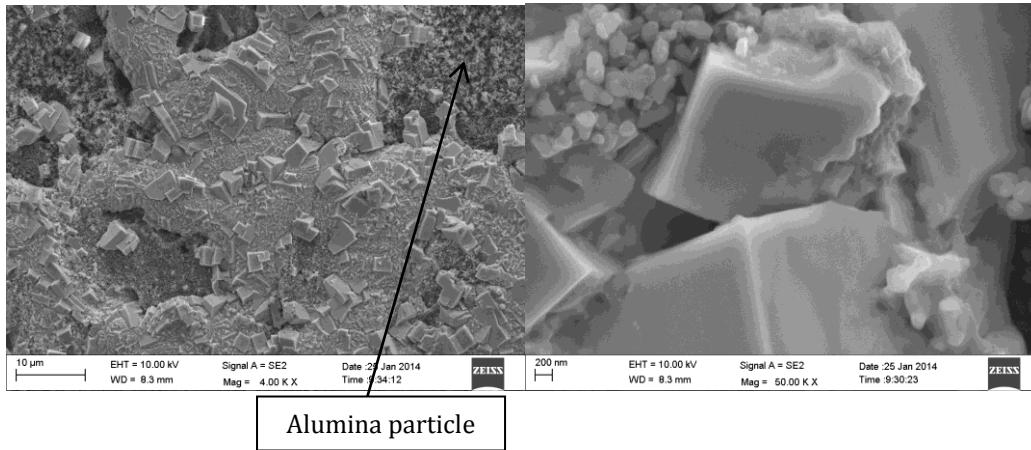


Figure 4-21: SEM micrographs of Cu+ 5wt% coarse Al₂O₃ after sintering

4.3.4 Density Measurement

The percentage relative density at each stage of processing is listed in the table 4-3.

Table 4-3: Percentage relative densities of PLD sample at each processing stage

	Cu + 5wt% coarse Al ₂ O ₃
Precompaction	60 %
CIP	73 %
Sintering	95 %

4.4 Deposition

Figure 4-17 depicts the photograph of PLD of samples. The green color laser plume is observed during the deposition from the target.

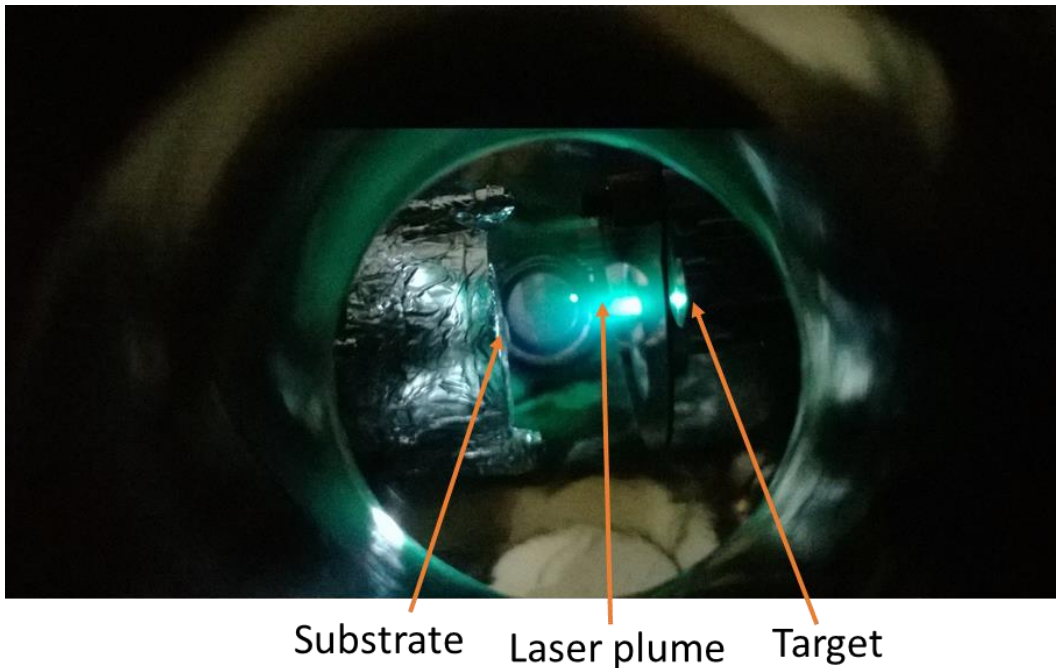


Figure 4-22: Photograph of PLD of Cu+5wt% coarse Al₂O₃

The figure 4-23 represents the photograph of the deposited film of Cu + 5wt% Al₂O₃.



Figure 4-23: Photograph of deposited film

It is observed that the film has grown on alumina substrate with average grain size of 7 microns. The table 4-4 represent the elemental composition of the film grown through EDS.

Table 4-4: Elemental Composition of deposited film

Element	Weight %	Atomic %
O K	0.99	48.19
Al K	0.50	14.39
Cu L	3.05	37.42

The figure 4-20 shows the SEM micrograph after of ablated region on the target. The figure 4-21 depicts the ablated ring formed on the target after PLD. The elemental composition of ablated and unablated region on the target is analyzed through EDS. Elemental composition of Ablated and unablated region is tabulated in table 4-5.

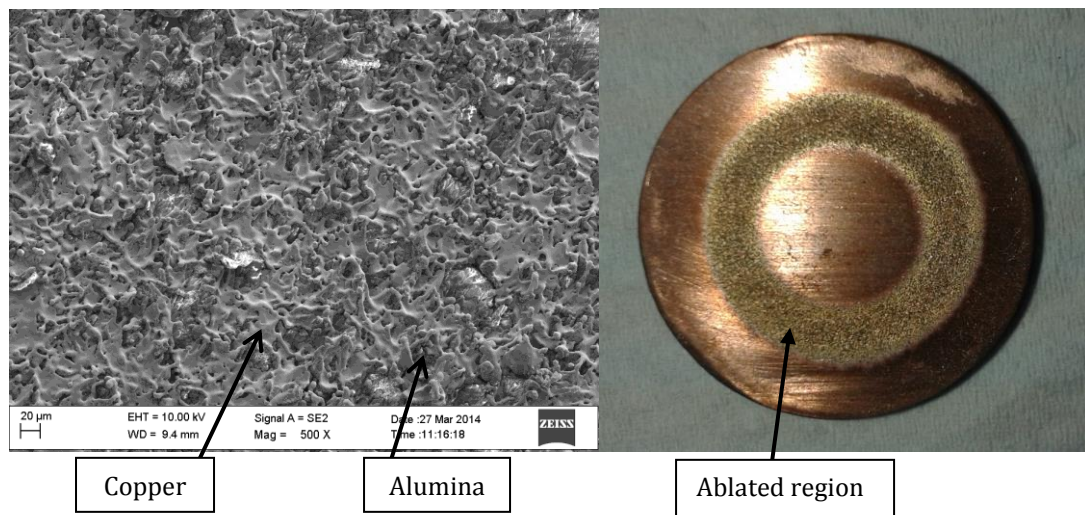


Figure 4-24 & 4-25: SEM micrograph of ablated region and photograph of target after PLD

Table 4-5: Elemental composition of ablated and unablated region

Element	Ablated region		Unablated region	
	Weight %	Atomic %	Weight %	Atomic %
O K	0.61	24.72	1.04	26.91
Al K	0.65	15.63	0.86	13.2
Cu L	5.81	59.65	9.2	59.89

The consolidated XRD plot of as received copper powder, sintered sample after TPM and deposited film shown in figure 4-26. The Cu_2O peaks are

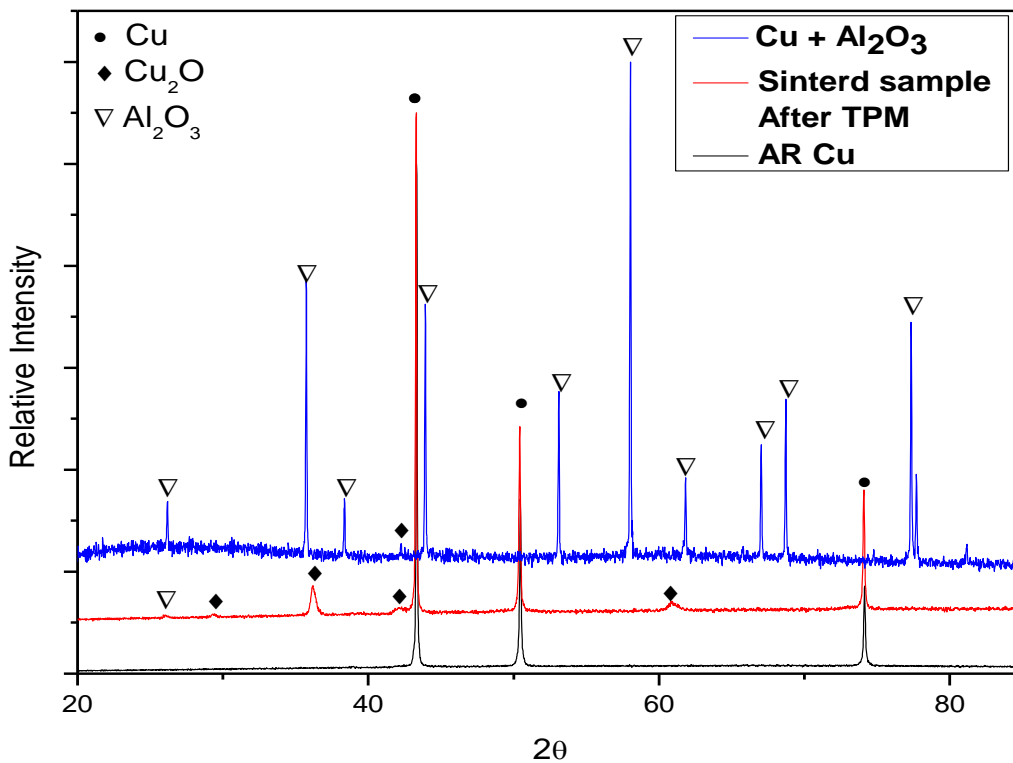


Figure4-26: XRD plot of as received copper, sintered sample of Cu+5wt% coarse Al₂O₃ after thermopower measurement, deposited film

confirmed with its JCPDS no 782076. After the TPM, Cu₂O peaks are detected in the sintered sample. Also the small Cu₂O peaks are detected in the thin film. The majority of the phase in thin film is Al₂O₃.

4.5 Discussion

The effect of particle size of alumina on the thermoelectric properties of Cu-Al₂O₃ composite is evident through the figure 4-13, 4-14, 4-15, 4-16, 4-17 and 4-18. The composite with fine alumina exhibit high resistivity as compared to composite with coarse alumina. Increase in the resistivity may be attributed to increased probability of electron being scattered from finer alumina particles at the interface. As the electron are being more dominantly scattered at the interface, finer alumina particles disrupt the net electron transport more dominantly than coarser alumina particles because of large interface area, resulting the composite with fine alumina particles to have higher resistivity ($\sim 10^{-7}$ ohm-m at room temperature to $\sim 10^{-6}$ ohm-m at 500 °C) as compared to composite with coarser particles ($\sim 10^{-8}$ ohm-m at room temperature to $\sim 10^{-7}$ ohm-m at 500 °C). Also with increase in temperature the electron scattering by phonon becomes prominent which results it into increase in resistivity. At 500 °C sudden increase in the Seebeck coefficient is observed in both types of composite. The sudden increase in Seebeck coefficient may be ascribed to oxidation of copper at higher temperature.

Copper oxides (Cu_2O) are semiconducting in nature [13]. The semiconductors have lower charge carrier density, as a consequence, the Seebeck coefficient tend to increase. The negative Seebeck coefficient of composite with fine alumina particles may be due to the electron as major carrier whereas the positive Seebeck coefficient of composite with coarse alumina particle may be due to the holes as charge carriers. Composite with finer alumina particles have higher Seebeck coefficient at $500\text{ }^{\circ}\text{C}$ ($-60\text{ }\mu\text{V/K}$). After analysis of elemental composition of thin film and target, there is profound reduction in atomic percent of copper being deposited. Reduction in the elemental composition of copper on film may be attributed to the outward flight of heavier element in the laser plume. Copper is heavier than aluminum and oxygen, as a result, reduction in atomic fraction of copper as compared to other elements.

Chapter 5

Summary

In the present work, the Seebeck coefficient and resistivity measurement of Cu+5wt% coarse Al₂O₃ and Cu+5wt% fine Al₂O₃ has been carried out at different temperature. Lower particle size of alumina increases resistivity of composite. At higher temperature oxidation of copper can increase the Seebeck coefficient due to the semiconducting properties of copper oxide. The copper oxides improve the thermoelectric properties of composite. The thermopower factor of composite with fine alumina is more because of higher Seebeck coefficient.

Chapter 6

Future Work

- Measurement of thermal conductivity of Cu+5wt% coarse Al₂O₃ and Cu+5wt% fine Al₂O₃ and consequently the figure of merit.
- Measurement of thermoelectric properties (electrical conductivity, thermal conductivity and Seebeck coefficient) of thin film and figure of merit.
- Study of effect of increasing amount of alumina on thermoelectric properties of the composite.

References

- [1] Rowe D. M., *CRC handbook of thermoelectrics*, 1995.
- [2] G. Chen, M. S. Dresselhaus, J. P. Fleurial, T. Caillat; *International Materials Review*. 48, 45, 2003.
- [3] H. Julian Goldsmid; *Introduction to Thermoelectricity*, Springer series in Materials Science, 2010.
- [4] Kasap O. S.; *Principles of Electronic Materials and Devices*; McGraw Hill publication; 3rd edition, 2006.
- [5] G. Jeffrey Snyder, Eric S. Toberer; *A Review Article: Complex thermoelectric materials*; *Nature materials*, Vol 7, 105, 2008.
- [6] Jin-cheng Zheng; *Recent advances on thermoelectric materials*; *Front. Phys. China*, 2008.
- [7] J.P. Heremans; *Low dimensional thermoelectricity*; *Acta Physica Polonica A*, Vol. 108, 2005.
- [8] Gregory et.al; *Nano-composite for thermal barrier coatings and thermoelectric energy generators*; *US patent application US2009/0290614A1*, 2009.
- [9] Anish Upadhaya, G.S. Upadhaya; *Sintering of copper-alumina composites through blending and mechanical alloying powder metallurgy routes*; *Materials & Design* Vol 16 1; 41-45; 1995.
- [10] Thomas Twardowski; *Introduction to nanocomposites materials: properties, processing and characterization*; *DEStech Publication*; 2007.
- [11] C. Suryanarayana; *Mechanical Alloying and Milling*; *Marcel Dekker*; 2004.
- [12] Cardelli Francois; *Materials handbook*; *Springer*; 2008.
- [13] Kenneth I. Hardee, Allen J. Bard; *Photoelectrochemical Behavior of Several Polycrystalline Metal Oxide Electrodes in Aqueous Solutions*; *Journal of Electrochemistry Society*; 1977.